



THE UNIVERSITY *of* EDINBURGH

Edinburgh Research Explorer

The Impact of Solar Irradiance on Visible Light Communications

Citation for published version:

Islim, MS, Videv, S, Safari, M, Xie, E, McKendry, JJD, Dawson, MD & Haas, H 2018, 'The Impact of Solar Irradiance on Visible Light Communications', *Journal of Lightwave Technology*, vol. 36, no. 12, pp. 2376 - 2386. <https://doi.org/10.1109/JLT.2018.2813396>

Digital Object Identifier (DOI):

[10.1109/JLT.2018.2813396](https://doi.org/10.1109/JLT.2018.2813396)

Link:

[Link to publication record in Edinburgh Research Explorer](#)

Document Version:

Peer reviewed version

Published In:

Journal of Lightwave Technology

General rights



Copyright for the publications made accessible via the Edinburgh Research Explorer is retained by the author(s) and / or other copyright owners and it is a condition of accessing these publications that users recognise and abide by the legal requirements associated with these rights.

Take down policy

The University of Edinburgh has made every reasonable effort to ensure that Edinburgh Research Explorer content complies with UK legislation. If you believe that the public display of this file breaches copyright please contact openaccess@ed.ac.uk providing details, and we will remove access to the work immediately and investigate your claim.



The Impact of Solar Irradiance on Visible Light Communications

Mohamed Sufyan Islam , *Graduate Student Member, IEEE*, Stefan Videv, Majid Safari, *Member, IEEE*, Enyuan Xie , Jonathan J. D. McKendry, Erdan Gu, Martin D. Dawson, *Fellow, IEEE*, and Harald Haas, *Fellow, IEEE*

Abstract—This paper aims to address the perception that visible light communication (VLC) systems cannot work under the presence of sunlight. A complete framework is presented to evaluate the performance of VLC systems in the presence of solar irradiance at any given location and time. The effect of solar irradiance is investigated in terms of degradations in signal to noise ratio, data rate, and bit error rate. Direct current (DC) optical orthogonal frequency division multiplexing is used with adaptive bit and energy loading to mitigate DC wander interference and low-frequency ambient light noise. It was found that reliable communication can be achieved under the effect of solar irradiance at high-speed data rates. An optical bandpass blue filter is shown to compensate for half of the reduced data rate in the presence of sunlight. This work demonstrates data rates above 1 Gb/s of a VLC link under strong solar illuminance measured at 50350 lux in clear weather conditions.

Index Terms—Light fidelity (LiFi), OFDM, solar irradiance, visible light communication (VLC).

I. INTRODUCTION

TRAFFIC from wireless and mobile devices will account for two-thirds of the total internet traffic by 2020 [1]. The radio frequency (RF) bandwidth is a scarce resource costing above \$1.28m per 1 MHz in the 2.4 GHz frequency band in the UK [2]. Visible light communication (VLC) offers a much larger frequency bandwidth that is unlicensed and safe to use. VLC has the potential to reuse the existing lighting infrastructure based on light emitting diode (LED) for communications purposes [3]. Light fidelity (LiFi) is the network solution for VLC that is proposed to work seamlessly beside other RF access technologies [3]. A record data rate of 7.91 Gb/s was reported

Manuscript received August 31, 2017; revised January 22, 2018; accepted February 25, 2018. This work was supported by the UK Engineering and Physical Sciences Research Council under Grants EP/K008757/1, EP/K00042X/1, and EP/M506515/1. This paper was presented in part at the IEEE International Symposium on Personal, Indoor and Mobile Radio Communications, Montreal, QC, Canada, October 2017. (*Corresponding author: Mohamed Sufyan Islam.*)

M. S. Islam, S. Videv, M. Safari, and H. Haas are with the Institute for Digital Communications, Li-Fi R&D Centre, The University of Edinburgh, Edinburgh EH9 3JL, U.K. (e-mail: m.islim@ed.ac.uk; s.videv@ed.ac.uk; m.safari@ed.ac.uk; h.haas@ed.ac.uk).

E. Xie, J. J. D. McKendry, E. Gu, and M. D. Dawson are with the Institute of Photonics, University of Strathclyde, Glasgow G1 1RD, U.K. (e-mail: enyuan.xie@strath.ac.uk; jonathan.mckendry@strath.ac.uk; erdan.gu@strath.ac.uk; m.dawson@strath.ac.uk).

Color versions of one or more of the figures in this paper are available online at <http://ieeexplore.ieee.org>.

Digital Object Identifier 10.1109/JLT.2018.2813396

for orthogonal frequency division multiplexing (OFDM)-based VLC using single violet micro-scale GaN led (micro-LED) [4]. Data rates above 100 Gb/s can be achieved when the complete visible spectrum is utilized [5].

The effect of solar irradiance is considered to be one of the main misconceptions surrounding VLC [6]. It is generally assumed that it could halt the operation of the communication system entirely due to interference. However, the effect of solar irradiance is more apparent as a strong shot noise source rather than an interference source as the sunlight intensity does not vary greatly over short periods of time. This allows multicarrier schemes such as OFDM to allocate the symbols over the usable frequency subcarriers of the deployed bandwidth [7].

The effect of solar irradiance on the performance of optical wireless communications (OWC) and VLC has been investigated in a limited number of works in the literature [8]–[12]. A simplified model was adopted in some of these works by approximating the solar irradiance to a black body radiation [8]. Other works adopted a standardized solar irradiance model [13] that is being used as a reference model in the research on solar energy harvesting [9]. However, the location and time of the studied system play important roles in characterizing the solar irradiance effect on VLC system performance. These important parameters were considered using computer simulation in [10]. However, the direct solar irradiance was not used to characterize the system performance. The solar irradiance was assumed to be incident from a window and reflected on multiple walls before it is collected by the photoreceivers. The impact of solar irradiance on the performance of underwater OWC links was investigated for positive-intrinsic-negative (PIN), avalanche photodiode (APD) and photomultiplier tube (PMT) using Monte Carlo simulation in [9]. It was shown that sunlight degrades the system performance at relatively low depths below 80 meters.

The use of optical filters with a light control film to mitigate the effects of sunlight was proposed in [8], [11]. A filter with a light control film called microlouver is used to restrict the field of view (FOV) and to reduce the background light collected at the photoreceiver. However, the light control film can not adapt to the changes of the photoreceiver orientation and location which limits the solution to fixed point-to-point systems. The objective of this paper is to provide a theoretical and experimental characterization of the solar irradiance effect on high-speed OFDM-based VLC systems. The investigation compares the use of a bandpass optical blue filter to the case where

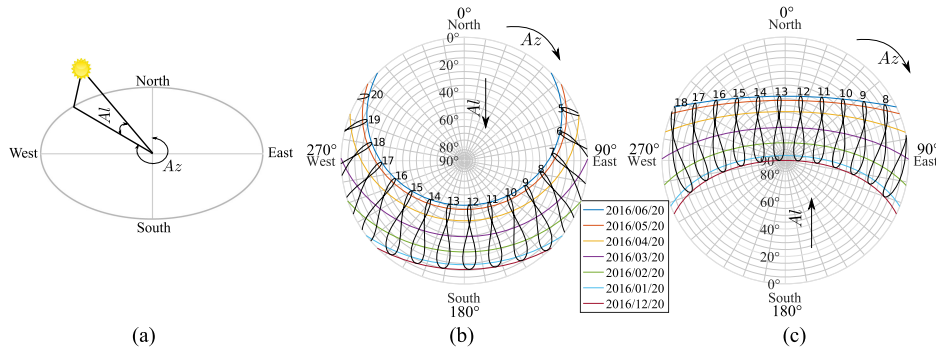


Fig. 1. (a) Solar position described by altitude and azimuth. (b) and (c) Solar position at Edinburgh and Antofagasta, respectively, for each 20th day of each considered month. The time of the day is listed above the elliptical shapes representing the Analemma diagrams.

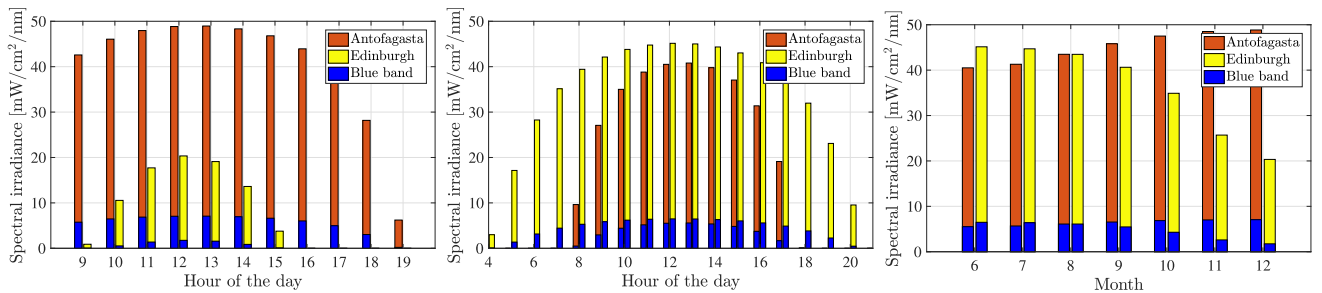


Fig. 2. Total solar irradiance estimated at Antofagasta and Edinburgh on the 20th of December 2016 (left) and on the 20th of June 2016 (center); and at the noon of each 20th day of the second half of the year (right). The blue spectral component of the solar irradiance is shown in blue.

80 a filter is not considered in front of the photoreceiver. The per-
 81 formance is compared to a benchmark scenario of a dark room
 82 where background light does not reach the photoreceiver.

83 In our previous work [14], we investigated the solar irradiance
 84 effect on VLC in Antofagasta, Chile based on worst-case
 85 scenarios in terms of location, link orientation and choice of
 86 photoreceiver. In this paper, we present a complete framework
 87 to investigate the sunlight effect on VLC at any given location
 88 and time. The previous literature were manily based on pulsed
 89 modulation techniques [11], [12]. However, an outdoor under-
 90 water VLC demonstration achieving a data rate of 58 Mb/s was
 91 considered using discrete multi-tone (DMT) [15]. In this work,
 92 we demonstrate our results by an experimental proof of concept
 93 of a high speed OFDM-based VLC system in Edinburgh,
 94 UK achieving data rate above 1 Gbps in the presence of solar
 95 irradiance without any optical filtering. The simulation and ex-
 96 perimental results show that the solar irradiance affects VLC
 97 link performance, but the effects are gradual and depend on a
 98 number of other parameters such as link margin. The simulation
 99 results show that at least half of the losses in data rate per-
 100 formance can be recovered using an inexpensive commercially
 101 available bandpass blue filter.

102 The rest of this paper is organized as follows. In Section II,
 103 we review the solar position and irradiance calculations based
 104 on location and time and present the results of two geographical
 105 locations. The assumptions of the theoretical study are specified
 106 in Section III-A. The signal-to-noise ratio (SNR), the maximum
 107 theoretical limit to the data rate and bit error rate (BER) of the
 108 system are derived and the system modelling is discussed in
 109 Section III-B. An experimental proof-of-concept is presented in

Section IV. The system performance is analyzed and the results
 are shown in Sections III-C and IV-B. Section V concludes the
 paper.

113 II. SOLAR IRRADIANCE AND POSITION 114

115 The solar constant flux density P_{SC} is given as 1366.1 W/m^2
 116 outside the Earth's atmosphere by the American society for
 117 testing and materials (ASTM) standard (ASTM E-490) [16].
 118 The solar irradiance is not limited to the visible spectrum as
 119 it spans the wavelengths from 250 nm to 2500 nm. The solar
 120 irradiance at different wavelengths is non-equally attenuated as
 121 it travels through the atmosphere due to the different absorption
 122 and scattering effects of the air molecules and aerosols. The
 123 shortest path for the sunlight exists when the Sun is located at
 124 the zenith point (imaginary point above the head of the observer).
 125 The optical air mass (AM) is approximated as the ratio of the
 126 actual sunlight path to the minimum path at the zenith point.
 127 It is given as AM0 for the extraterrestrial irradiance. When the
 128 Sun is at angle θ_Z relative to the zenith, the optical AM is
 approximated as:

$$AM \simeq \frac{1}{\cos \theta_Z}. \quad (1)$$

129 The solar irradiance at $\theta_Z = 48.2^\circ$ is given at an AM1.5 by the
 130 standard (ASTM E-490) [13] as a reference to help the solar
 131 energy community in testing and comparing the performance of
 132 various solar cells. However, the solar irradiance varies based
 133 on the geographical location; seasonal and diurnal variations
 134 arising from the rotation of the Earth around the Sun; and the

TABLE I
MODELLING ASSUMPTIONS

Locations	Edinburgh, UK, 55°55'20.4"N 3°10'23.3"W Antofagasta, Ch, 23°27'16.1"S 70°26'21.4"W
Dates	Every 20 th of each considered month
APD model	Hamamatsu S8664-50K
APD detection area, A	19.6 mm ²
Bandwidth, B	60 MHz
APD gain, M	100
Dark current, I_d	3 nA
Blue filter FWHM	50 nm
Maximum transmitted optical power, P_{Max}^L	8 mW
Transmission distance, d	63.85 cm
Half-power semi-angle of the transmitter, $\Phi_{1/2}$	25°

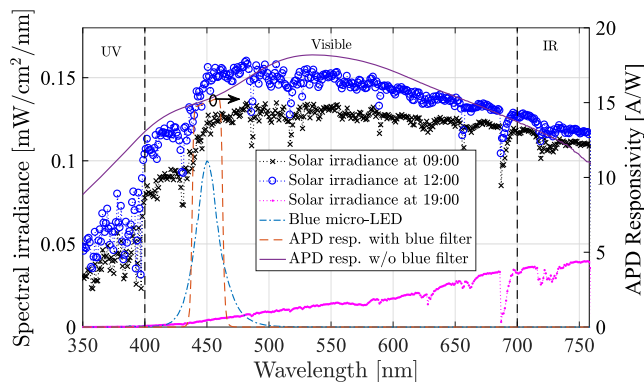


Fig. 3. The predicted solar irradiance in Antofagasta at 9 AM, 12 PM and 19 PM (local time) of the 20th on December 2016 (left), alongside the spectral irradiance of the modeled micro-LED centred at 450 nm (left) and response of the APD with and without considering the transmittance of the blue filter (right).

135 rotation of the Earth around its own axis. The effect of solar irradiance on VLC varies based on the location and time. Therefore, 136 it is essential to calculate the position of the Sun in the sky in order for the solar irradiance at a particular location and time 137 to be estimated. Various algorithms with different complexities and accuracies for calculating the solar position exist in the as- 138 trophysics literature [17]. In Appendix A, we review a simple 139 algorithm based on the ecliptic coordinates with an accuracy 140 of $(1/60)^\circ$ presented in [18] and proposed by the astronomical 141 applications department of the U.S. naval observatory [19]. 142

143 The horizontal coordinate system is usually used for solar 144 energy applications where the horizon of the observer is con- 145 sidered to be the fundamental plane. The solar position can be 146 described using two angles: altitude Al and azimuth Az . The 147 solar altitude $Al \in [0^\circ, 90^\circ]$ is given as the elevation of the Sun 148 above the horizon. A solar altitude of $Al = 90^\circ$ means that the 149 Sun is at the zenith point. The solar altitude can also be given as 150 $Al = 90^\circ - \theta_z$. The solar azimuth $Az \in [0^\circ, 360^\circ]$ is given as 151 the angle between the north and the horizontal projection of the 152 line-of-sight (LoS) between the Sun and the observer. Both an- 153 gles are illustrated in Fig. 1(a) and demonstrated in Fig. 1(b) and 154 (c) for Edinburgh, UK and Antofagasta, Chile on the 20th of each 155 considered month, respectively. The solar altitude is shown to 156 reach the zenith $Al = 90^\circ$ around 13:00 on the 20th of December 157 158

2016 for Antofagasta in Fig. 1(c). The time of the day is shown 159 above the analemma diagrams in Fig. 1(b) and (c), which depict 160 the Sun's motion throughout the year when observed at the same 161 location and the same hour of day. 162

163 Direct solar irradiance is the sunlight that is directly reaching 164 the surface of the Earth. Global solar irradiance is the combina- 165 tion of the direct and diffused solar irradiance. The simple model 166 of the atmospheric radiative transfer of sunshine (SMARTS) is 167 a transmittance model to evaluate the direct solar irradiance at 168 any particular location and time [20], [21]. The model is used 169 in generating the ASTM standard (ASTM E-490) with a reso- 170 lution of 0.5–1 nm [16]. The direct solar irradiance is typically 171 stronger than the signal of interest when the total solar irradiance 172 is taken into account. Fortunately, VLC is realized using mono- 173 chromatic or multi-chromatic optical sources that has fixed and 174 pre-defined spectral irradiance. This allows inexpensive com- 175 mercially available optical filters to be a practical solution for 176 the degradations caused by solar irradiance. The total predicted 177 solar irradiance is shown in Fig. 2(a) and (b) for Antofagasta 178 and Edinburgh at the noon of December and June solstices, re- 179 spective. Monthly comparisons for the total solar irradiance 180 are shown in Fig. 2(c). The total spectral irradiance is calculated 181 for the visible spectrum between 400 nm and 760 nm. The blue 182 component of the solar irradiance for the wavelengths between 183 425 nm and 475 nm shows the importance of optical filtering 184 in improving the VLC communications performance. Optical 185 filtering is also beneficial for other objectives in VLC. White il- 186 lumination is generally achieved by coating the blue LED with 187 a yellow phosphor which introduces a slow component into the 188 frequency response of the LED. Blue filters are required to 189 eliminate the slow response component of the yellow phos- 190 phor. Monochromatic light sources with narrowband spectral 191 distributions can guarantee a robust VLC system against solar 192 irradiance with the potential of achieving data rates in the orders 193 of multiple Gb/s.

III. THEORETICAL STUDY 194

A. Modelling Assumptions 195

196 An OFDM-based VLC system is assumed due to its robust- 197 ness against background illumination flickering. The OFDM 198 waveform is required to be both unipolar and real valued. Her- 199 mitian symmetry is imposed on the M -ary quadrature amplitude 200 modulation (M -QAM) symbols, to enforce the OFDM time do- 201 main signal output into the real domain. This can be written as: 202 $X[k] = X^*[N_{FFT} - k]$, where N_{FFT} is the OFDM frame size. 203 The subcarriers $X[0]$ and $X[N_{FFT}/2]$ are both set to zero. A 204 real-valued OFDM waveform with a direct current (DC) bias is 205 used to modulated the intensity of the LED in what is known 206 as DC-biased optical OFDM (DCO-OFDM). Binary inputs are 207 encoded into multiple M -QAM symbols which are allocated 208 into N_{FFT} subcarriers over a single-sided bandwidth of B . DC 209 bias is used to shift the negative signal samples into positive 210 values. Three scenarios are considered: 210

- *Dark room (Scenario 1)*: assumes an optimal case where 211 no background illumination is reaching the photoreceiver. 212

213 This is an ideal scenario as the dominant noise source is
214 the thermal noise.

- 215 • *With blue filter (Scenario II)*: assumes that the solar irra-
216 diance is collected with a bandpass blue filter in front of
217 the photoreceiver. This is a practical scenario as the useful
218 transmitted signal is passed and any out-of-band signal is
219 filtered. Part of the solar irradiance is passed since it covers
220 a wide wavelength band.
- 221 • *Without blue filter (Scenario III)*: assumes a worst case
222 scenario where the solar irradiance is collected without
223 any optical filtering in front of the photoreceiver.

224 The modeling assumptions are presented in Table I. The sys-
225 tem uses a blue micro-LED with a pixel size of $100 \times 100 \mu\text{m}^2$
226 and a maximum optical power of 8 mW. Due to the reduced
227 emission area of micro-LEDs, the capacitance decreases and
228 current density increases allowing for higher 3-dB bandwidths
229 compared to off-the-shelf LEDs [22]. The transmission distance
230 is specified at $d = 63.85$ cm to match with the distance that
231 we have used to measure the spectral irradiance of the micro-
232 LED. The system performance is also investigated at longer
233 distances up to 3 meters in Section III-C. A focusing aspheric
234 condenser optical lens (Thorlabs, ACL4532U-A) is used at the
235 transmitter side, which allows for a small half-power semi-angle
236 at the transmitter $\Phi_{1/2} = 25^\circ$. An optical bandpass blue filter
237 from Edmund Optics is assumed in Scenario II with a center
238 wavelength of 450 nm, a transmittance higher than 90%
239 and a full width at half maximum (FWHM) of 50 nm. The
240 photoreceiver is an APD (Hamamatsu, S8664-50K) where it is
241 assumed to be aligned with the micro-LED. APDs operate at
242 high reverse bias to create an amplification effect that allows
243 incident photons to create an avalanche of electrons. APDs are
244 more sensitive to background noise compared to other photo-
245 diodes. However, APDs are used as a worst case choice in this
246 investigation as they are shot-noise limited [23]. The APD will
247 not always be collecting the solar irradiance due to the orienta-
248 tion of the communication link in practical situations. However,
249 the APD is always assumed to be collecting the sunlight in this
250 investigation.

251 The locations considered are $55^\circ 55' 20.4''\text{N}$ $3^\circ 10' 23.3''\text{W}$ in
252 Edinburgh, UK and $23^\circ 27' 16.1''\text{S}$ $70^\circ 26' 21.4''\text{W}$ in Antofa-
253 gasta, Chile. The former location is used to compare with the
254 experimental results and the latter is claimed to have the highest
255 solar radiation on Earth [24]. The model considers two dates:
256 summer solstice and winter solstice where the solar position
257 is calculated and used in SMARTS [20], [21] to estimate the
258 hourly solar irradiance data. The model assumes a clear sky
259 scenario due to the irregular variations in the local weather con-
260 ditions which influence the solar irradiance. This allows us to
261 consider the maximum possible solar irradiance in a pessimistic
262 approach. As the considered locations lies in the north and south
263 hemispheres, the summer solstice at Edinburgh would be winter
264 solstice at Antofagasta and similarly the opposite is true.

265 B. System Modeling

266 The OFDM waveform $x(t)$ is transmitted over the VLC chan-
267 nel $h(t)$, before it is distorted with noise $n(t)$ at the receiver.

268 The received signal $r(t)$ is then sampled at $1/T$ with an analog-
269 to-digital converter (ADC), where T is the sampling period. Fast
270 Fourier transform (FFT) is then applied on the samples after
271 serial to parallel (S/P) conversion. Assuming that the OFDM
272 frame size is large ($N_{\text{FFT}} > 64$) [25], central limit theorem
273 (CLT) can be applied on the combination of noise generated at
274 the receiver. This can be modeled as zero mean additive white
275 Gaussian noise (AWGN) with variance σ_n^2 . The received OFDM
276 waveform $r(t)$ can be given as:

$$r(t) = h(t) * x(t) + n(t). \quad (2)$$

277 The average photocurrent generated at the APD due to the
278 average optical power received from sunlight is given as:

$$I_b = A_d \int_{350}^{750} P_D^S(\lambda) R(\lambda) T_{\text{bf}}(\lambda) d\lambda, \quad (3)$$

279 where A_d is the APD detection area, $P_D^S(\lambda)$ is the direct solar
280 irradiance given in $\text{W}/\text{m}^2/\text{nm}$, $T_{\text{bf}}(\lambda)$ is the transmittance of the
281 bandpass optical blue filter, $R(\lambda)$ is the intrinsic responsivity of
282 the APD given in A/W and λ is the wavelength considered for
283 the visible light spectrum mainly from 350 nm to 750 nm.

284 Similarly, the average photocurrent generated at the APD due
285 to the average optical power received from the micro-LED is
286 given as:

$$I_x = \frac{(m+1)A_d}{2\pi d^2} \int_{350}^{750} P_T^L(\lambda) R(\lambda) T_{\text{bf}}(\lambda) d\lambda, \quad (4)$$

287 where $m = -1/\log_2(\cos(\Phi_{1/2}))$ is the Lambertian order of the
288 micro-LED; d is the Euclidean distance between the micro-LED
289 and the APD; and $P_T^L(\lambda)$ is the transmitted optical irradiance
290 from the micro-LED, which is given as:

$$P_T^L(\lambda) = P_{\text{Max}}^L \frac{P_{\text{Measured}}^L(\lambda)}{\int_{350}^{750} P_{\text{Measured}}^L(\lambda) d\lambda}, \quad (5)$$

291 where P_{Max}^L is the maximum transmitted optical power of the
292 micro-LED and $P_{\text{Measured}}^L(\lambda)$ is the measured optical irradiance
293 of the micro-LED given in $\text{W}/\text{m}^2/\text{nm}$. This was measured at a
294 distance of $d = 63.85$ cm using a Labsphere spectral irradiance
295 head (E1000).

296 The random arrival of incident photons results in shot noise
297 which can be modeled by a Poisson distribution. However, when
298 the number of incident photons increases, the shot noise is
299 approximated by a Gaussian distribution [26]. The shot noise
300 variance is given by [27]:

$$\sigma_s^2 = 2qM^2 F(I_b + I_x) B, \quad (6)$$

301 where M is the average gain of the APD, q is the electron charge,
302 B is the bandwidth of the APD and F is the excess noise given
303 as [28]:

$$F = \kappa M + (2 - 1/M)(1 - \kappa), \quad (7)$$

304 where κ is the holes/electrons ionization rate. The SNR at sub-
305 carrier k can be given by:

$$\gamma_k = \frac{M^2 I_x^2}{\sigma_n^2 / |H(k)|^2}, \quad (8)$$

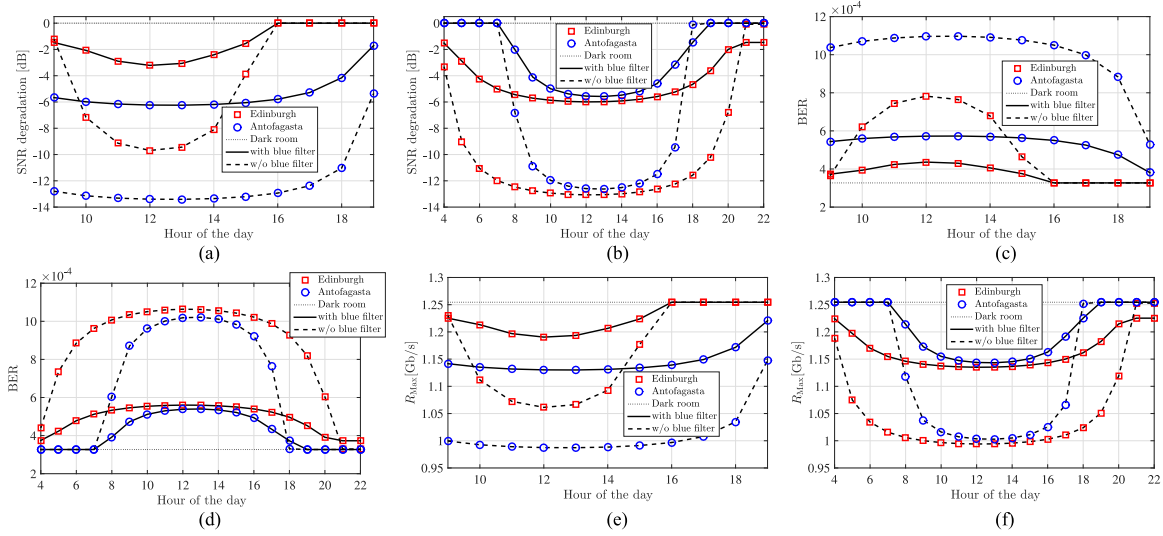


Fig. 4. (a and b) SNR; (c and d) BER; (e and f) maximum theoretical limit to the data rate. All results are presented for the three considered scenarios in Antofagasta and Edinburgh versus time at the 20th of December 2016 (a, c, e) and 20th of June 2016 (b, d, f).

306 where $H(k)$ is the frequency domain realization of the VLC
 307 channel, $\sigma_n^2 = \sigma_s^2 + \sigma_t^2 + \sigma_d^2$ and σ_d^2 is the variance of the dark
 308 noise which is given as [27]:

$$\sigma_d^2 = 2qM^2FI_{dg}B + 2qI_{ds}B, \quad (9)$$

309 where I_{ds} is the surface dark current and I_{dg} is the bulk dark
 310 current that experience the avalanche effect of the APD and
 311 where $I_d = I_{ds} + MI_{dg}$. The variance of the thermal noise σ_T^2
 312 is given by [29]:

$$\sigma_T^2 = 4 \left(\frac{K_B T}{R_L} \right) F_n B, \quad (10)$$

313 where K_B is Boltzmann constant, T is the temperature in
 314 Kelvin, R_L is the load resistance given as 50Ω and F_n is the
 315 photodiode noise figure.

316 Adaptive bit and energy loading algorithms such as the Levin-
 317 Campello algorithm [30] can be used to maximize the data rate
 318 by assigning larger constellation sizes on the subcarriers that
 319 have higher SNR. The maximum theoretical limit to the data
 320 rate of DCO-OFDM can be calculated using the channel capac-
 321 ity defined by Shannon-Hartley theorem [31] when neglecting
 322 the DC bias and the optical source nonlinearity [32]. This is
 323 given as:

$$R_{\text{Max}} = B \sum_{\substack{k=1 \\ M'_k > 0}}^{N_{\text{FFT}}/2-1} \log_2(1 + \gamma_k), \quad (11)$$

324 where M'_k is the constellation order of M'_k -QAM used at sub-
 325 carrier k .

326 The system performance in terms of BER can be calculated
 327 using the theoretical BER of real-valued OFDM given for fre-
 328 quency selective channels [33]. The BER at subcarrier k can be

given as:

$$\text{BER}(M'_k, \gamma_k) \cong \frac{4}{\log_2(M'_k)} \left(1 - \frac{1}{\sqrt{M'_k}} \right) \times \sum_{l=1}^R Q \left((2l-1) \sqrt{\frac{3\gamma_k}{2(M'_k - 1)}} \right), \quad (12)$$

330 where $Q(\cdot)$ is the complementary cumulative distribution
 331 function (CCDF) for the standard normal distribution and
 332 $R = \min(2, \sqrt{M'_k})$. The overall system BER can be given as:

$$\text{BER} = \frac{\sum_{\substack{k=1 \\ M'_k > 0}}^{N_{\text{FFT}}/2-1} \text{BER}(M'_k, \gamma_k) \log_2(M'_k)}{\sum_{\substack{k=1 \\ M'_k > 0}}^{N_{\text{FFT}}/2-1} \log_2(M'_k)} \quad (13)$$

C. Results and Discussions

333 The spectral irradiance of the micro-LED and the amplified
 334 responsivity of the APD $MR(\lambda)$ are shown in Fig. 3 with the
 335 presence and absence of the optical bandpass blue filter. In addition,
 336 the predicted spectral irradiance of the sunlight at Antofa-
 337 gasta is shown at three different times of the summer solstice.
 338 It is shown that the solar irradiance is high at the ultra-violet
 339 (UV) and blue spectrum bands at sunrise. At sunset it becomes
 340 higher at the red and infra-red (IR) spectrum bands. The blue
 341 filter captures 70% of the micro-LED irradiance.
 342

343 The system performance is presented in Fig. 4(a) and (b) as
 344 a function of the SNR degradation against the time of the day
 345 for both December and June solstice, respectively. The degrada-
 346 tion is calculated with reference to the benchmark case of the
 347 dark room in Scenario I. It is shown that the SNR degrades
 348 by a maximum of -13.4 dB and -9.69 dB at the noon of De-
 349 cember solstice in Scenario III at Antofagasta and Edinburgh,
 350 respectively. However, when a blue filter is used in front of the

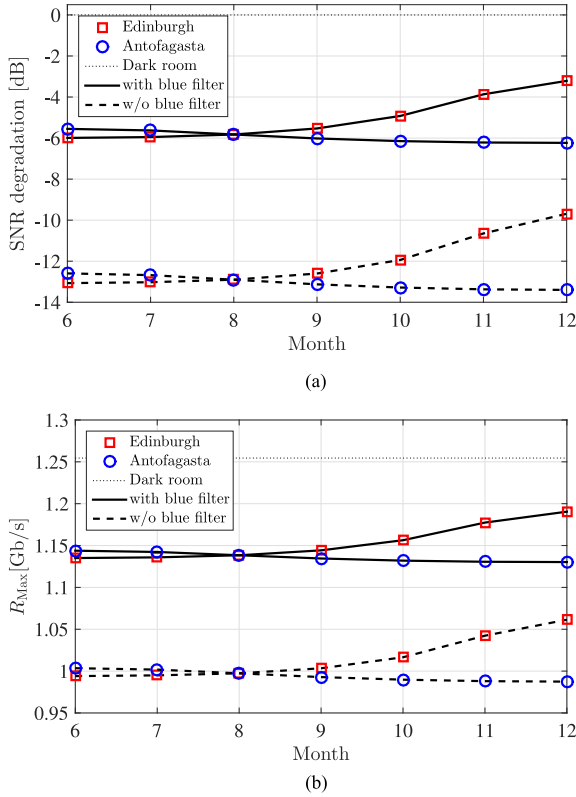


Fig. 5. The system performance presented on monthly basis at the noon of each 20th day of the considered months for the three considered scenarios in Antofagasta and Edinburgh. (a) SNR and (b) Maximum theoretical limit on data rate.

351 APD, this degradation is reduced to -6.23 dB and -3.214 dB
 352 in Scenario II at Antofagasta and Edinburgh, respectively. The
 353 high degradation in SNR at Antofagasta is expected due to the higher
 354 solar irradiance in December solstice in comparison with
 355 Edinburgh as shown in Fig. 2(a). The SNR degradations at Ed-
 356 inburgh for June solstice increase in comparison with December
 357 solstice by a maximum increase of 3.38 dB. The SNR degrada-
 358 tion is 0.8 dB lower for June solstice compared with December
 359 solstice at Antofagasta. A minimum of 6.47 dB improvement in
 360 SNR is achieved when blue filters are used in Scenario II. The
 361 SNR degradation at Edinburgh are witnessed for longer hours
 362 during June solstice due to the longer daylight that is shown in
 363 Fig. 1(b). The SNR degradation at Antofagasta and Edinburgh
 364 at the 20th day of the noon of the last six months of 2016 is
 365 presented in Fig. 5(a). The degradation decreases noticeably as
 366 we approach December solstice at Edinburgh, while SNR
 367 degradation variations are less noticeable for Antofagasta.

368 The system performance as a function of the BER against
 369 the time of the day is shown in Fig. 4(c) and (d) for 128-QAM
 370 DCO-OFDM at December and June solstices, respectively. The
 371 results show the SNR degradation effect on the BER perfor-
 372 mance for the OFDM-based VLC system. Both scenario II and
 373 scenario III at Antofagasta and Edinburgh are shown to allow
 374 the use of forward error correction (FEC) in both December and
 375 June solstice, although a significant improvement is shown to be
 376 achieved when the blue filter is used. The system performance

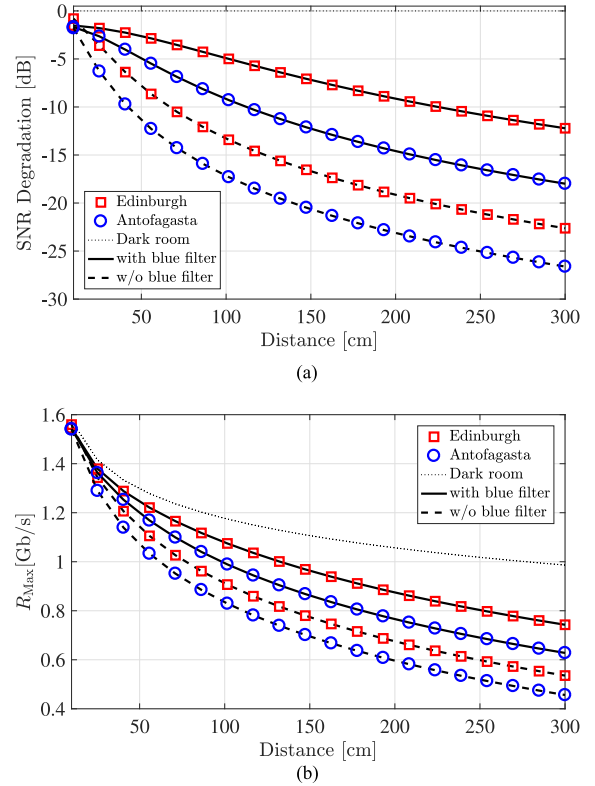


Fig. 6. System performance versus transmission distance d at the noon of the 20th of December 2016 for the three considered scenarios in Antofagasta and Edinburgh. (a) SNR and (b) Maximum theoretical limit on data rate.

is investigated as a function of the maximum theoretical limit to
 the data rate versus the time of the day in Fig. 4(e) and (f) for
 December and June solstices, respectively. The performance of
 Scenario II and the performance of Scenario III are compared to
 the benchmark performance recorded at 1.25 Gb/s of Scenario I
 for Antofagasta and Edinburgh. It is shown that the data rate
 degrades by 21.35% and by 15.49% at the noon of December
 solstice when the blue filter is not used in Antofagasta and Ed-
 inburgh, respectively. However, this degradation is reduced to 10%
 and 5.22% for Scenario II at Antofagasta and Edinburgh, respec-
 tively. This is equivalent to a significant 53.16% and 66.30%
 improvement that is achieved by placing a blue filter in front
 of the APD. A maximum theoretical limit to the data rate for
 June solstice under the solar irradiance is estimated at 1.03 Gb/s
 and 0.99 Gb/s for Scenario III at Antofagasta and Edinburgh,
 respectively and at 1.14 Gb/s and 1.13 Gb/s for Scenario II at
 Antofagasta and Edinburgh, respectively. A comparison of the
 maximum data rate performance at both Antofagasta and Ed-
 inburgh at noons of the last six months of 2016 is presented in
 Fig. 5(b). The variations in data rates are more noticeable for
 Edinburgh, where it increases to reach a maximum of 1.19 Gb/s
 for Scenario II and 1.06 Gb/s for Scenario III in December.

The SNR degradation and the maximum theoretical limit on
 the data rate are given in Fig. 6(a) and (b) as functions of the
 transmission distance. The results in Fig. 6 are presented for
 the three considered scenarios at Antofagasta and Edinburgh
 at noon of the 20th of December 2016. The SNR degrades as
 the transmission distance increases in all considered scenarios,

405 including the dark room scenario I, as expected. However, the
 406 SNR degradation for Scenario II and III are calculated with
 407 reference to the dark room in scenario I to highlight the solar
 408 irradiance effect in comparison with the benchmark Scenario I.
 409 It is shown that the SNR degradation reaches -26.61 dB and
 410 -22.63 dB when the blue filter is not used in Scenario III at a
 411 transmission distance of 3 meters at Antofagasta and Edinburgh,
 412 respectively. Although the SNR degradation appears to be high,
 413 the SNR gain of using the blue filter in Scenario II reaches
 414 8.6 dB and 10.41 dB at a transmission distance of 3 meters for
 415 Antofagasta and Edinburgh, respectively. Similarly, the maxi-
 416 mum theoretical limit on the data rate is shown to decrease as
 417 the transmission distance increases. The maximum theoretical
 418 limit on the data rate at a transmission distance of 3 meters for
 419 the dark room in Scenario I is 986.3 Mb/s. This is degraded
 420 by 53.74% for Antofagasta and 45.71% for Edinburgh in Sce-
 421 nario III. However, it is shown that the degradation is reduced
 422 to 36.33% and 24.7% in Antofagasta and Edinburgh when the
 423 blue filter is used in Scenario II. Despite the degradation in
 424 SNR, high-speed VLC can still be available at sufficiently long
 425 distances.

426 IV. EXPERIMENTAL STUDY

427 A. Experimental Set-Up

428 The measurements were conducted between 11:00–17:00 (lo-
 429 cal time) of the 6th and 9th of June 2016 under clear sky weather
 430 conditions demonstrated by very good visibility estimated
 431 above 21 km and a solar illuminance measured at 50350 lux.
 432 The measurements were carried at $55^{\circ}55'20.4''N$ $3^{\circ}10'23.3''W$
 433 in Edinburgh, UK. The experimental setup is shown in
 434 Fig. 7(a)–(b). The system elements used in the experiment
 435 are the same components described in Section III-A. The
 436 OFDM modulation waveform is generated and processed off-
 437 line using MATLAB. The OFDM digital waveform is con-
 438 verted into an analog waveform using the arbitrary waveform
 439 generator Agilent 81180A, which sends the bipolar OFDM
 440 waveform to the micro-LED using a Bias-Tee ZFBT-4R2GW.
 441 The DC bias is selected after exhaustive tests at $V_{DC} = 4.1$
 442 Volts to minimize the clipping distortion. The optical power
 443 of the micro-LED is 4.5 mW and the 3-dB bandwidth is
 444 30 MHz, both measured at DC current $I_{DC} = 50$ mA. An as-
 445 pheric collimation lens ACL 4532 is used to focus the light
 446 on the photoreceiver. Two Silicon APDs are used in this ex-
 447 periment (Hamamatsu, S8664-05k) and (Hamamatsu, S8664-
 448 50k), as shown in the top-right corner of Fig. 7(b). These
 449 APDs are referred to as ‘small’ APD and ‘large’ APD, respec-
 450 tively. The small APD has a smaller active area of 0.19 mm²
 451 and therefore, has a lower capacitance that leads to a higher
 452 3-dB bandwidth of 680 MHz. The large APD has a larger active
 453 area of 19.6 mm² that leads to a higher capacitance and lower
 454 3-dB bandwidth of 60 MHz.

455 The received signal at the APDs is filtered using a low
 456 pass electrical filter (Mini-circuits, SLP-100+) with a cut-off
 457 of 98 MHz for the large APD; and (Mini-circuits, SLP-250+)
 458 with a cut-off of 225 MHz for the small APD. Both filters are
 459 shown in Fig. 7(a). The system modulation bandwidth is used
 460 at 100 MHz and 250 MHz for the large and small APDs, re-

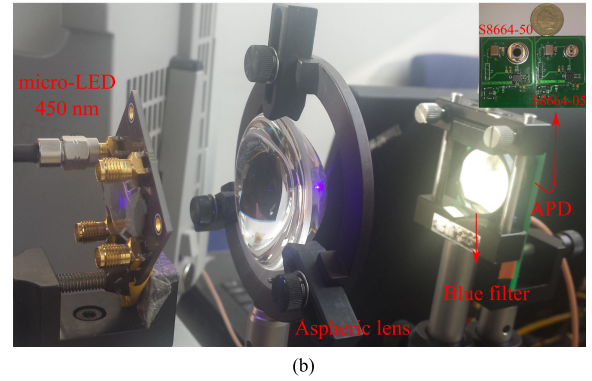
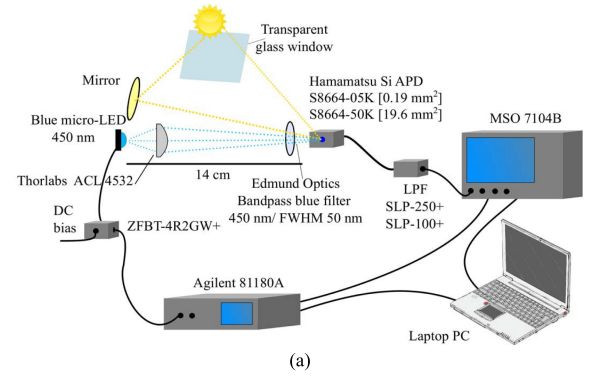


Fig. 7. The experimental set-up. (a) Schematic set-up of the experiment showing the optical system, arbitrary waveform function generator, oscilloscope, electrical and optical filters and Bias-T. (b) Photograph of the optical system showing the micro-LED, optical lenses system and the used APDs. In the top right corner (left): large APD s8664-50k; (right): small APD S8664-05k.

461 spectively. This is experimentally determined as the maximum
 462 bandwidth that allows for a SNR higher than 0 dB to be achieved.
 463 The electrical signal is then captured using an oscilloscope (Ag-
 464 ilent, MSO7104B) and then processed using MATLAB. The
 465 overall distance between the micro-LED and the photodetec-
 466 tor is 14 cm. The received optical power from the micro-LED
 467 would decrease at longer distances and consequently this would
 468 degrade the SNR because the SNR diminishes as the desired
 469 signal diminishes, but not because of noise due to sunlight. The
 470 distance is limited by the optical power of the micro-LED and
 471 it can be improved using more advanced collimation optics or
 472 using micro-LEDs with multiple pixels in a ganging mode [22].
 473 The three scenarios described in Section III-A are considered
 474 in the experimental study. The SNR of the channel is first esti-
 475 mated and then the constellation sizes and the associated power
 476 of M -QAM symbols are adaptively allocated to each subcar-
 477 rier based on the estimated SNR. The adaptive bit and energy
 478 loading algorithm avoids the use of low-frequency subcarriers,
 479 where the interference of ambient light can be strong. In addi-
 480 tion, it avoids any other subcarrier, where the SNR is expected
 481 to result in a BER below the FEC target.

482 B. Results and Discussions

483 The measured solar irradiance is given in Fig. 8 for the wave-
 484 lengths between 350 and 750 nm covering the visible spec-
 485 trum and part of the infrared and ultraviolet spectra. Four cases
 486 are presented: direct sunlight; reflected sunlight from a mirror,

TABLE II
ACHIEVABLE SNR VALUES AND DATA RATES FOR THE SMALL AND LARGE APDs FOR THE THREE CONSIDERED SCENARIOS

	Dark room (Scenario I)		with blue filter (Scenario II)		w/o blue filter (Scenario III)	
	Large APD	Small APD	Large APD	Small APD	Large APD	Small APD
Average SNR [dB]	17.57	18.58	16.64	17.36	12.42	16.42
Data rate @ BER<3.8e-3 [Mb/s]	416.44	1139.26	396.71	1080	313.35	1015

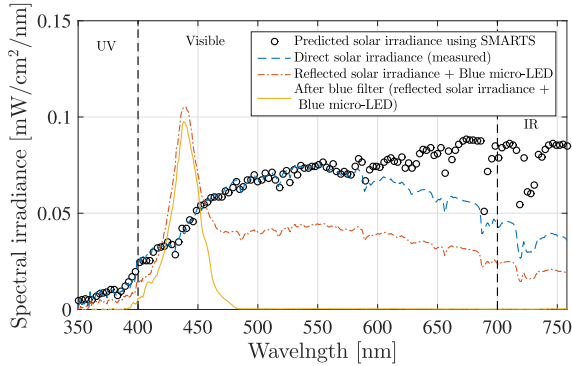


Fig. 8. The spectral distribution of the solar irradiance measured and predicted using SMARTS [20], [21] for Edinburgh (direct, reflected and filtered) in the presence and absence of the desired signal at 450 nm.

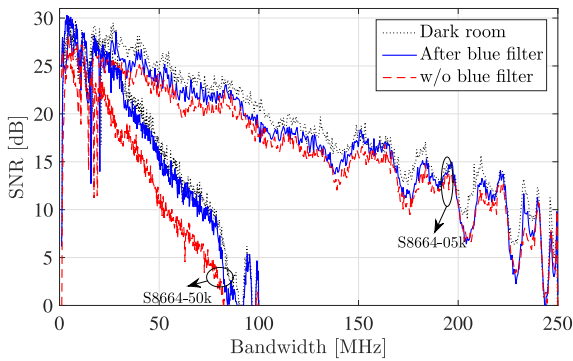


Fig. 9. Experimentally estimated SNR versus the system bandwidth when small and large APDs are used for the three considered scenarios.

487 reflected sunlight and blue micro-LED (Scenario III); and re-
 488 flected sunlight and blue micro-LED with a blue optical filter
 489 (Scenario II). The experiment was conducted inside a building
 490 where the direct sunlight is passed through a transparent glass
 491 window before it is collected at the photoreceiver. It was practi-
 492 cally infeasible to realize the experimental setup while the direct
 493 solar irradiance is always focused into the APD due to the vary-
 494 ing solar position throughout the experiment duration. A mirror
 495 was used to work around this issue at the expense of reduced so-
 496 lar irradiance. This was shown to have little impact on the blue
 497 band below 450 nm as it is shown in Fig. 8. The experimen-
 498 tally measured direct solar irradiance is shown to be identical
 499 to the simulated solar irradiance below 580 nm. The mismatch
 500 at longer wavelengths is attributed to the high reflectance and
 501 less transmittance characteristics of heat mirrors glazing in the
 502 infrared band that aim to improve building heat insulation [34].
 503 The experimentally estimated SNR is presented in Fig. 9
 504 for the small and large APDs at all the considered scenarios.
 505 All the performance comparisons are presented with reference
 506 to the optimal dark room (Scenario I). It is shown that the
 507 performance of the VLC system degrades in the presence of

508 direct sunlight for both APDs. The degradation in the average
 509 SNR is estimated at 2.16 dB for the small APD and 5.15 dB
 510 for the large APD in Scenario III. The photocurrents generated
 511 by both signal and background noise generally increase as the
 512 detection area of the APD increases. However, an optical source
 513 with small emission area and an imaging lens are used in this
 514 experiment to focus the light into the APD. The focused light
 515 spot size at the APD can ideally be as small as the emission
 516 area of the micro-LED (0.01 mm^2) [35]. Therefore, The signal
 517 photocurrent does not increase when the detection area becomes
 518 larger than the focused light spot at the APD. This validates the
 519 result that the SNR degradation is higher for the large APD,
 520 because it collects more background light. When the blue filter
 521 is used to restrict the unwanted irradiance, the degradation in
 522 the average SNR is reduced to 1.22 dB for the small APD
 523 and 0.93 dB for the large APD. Similar trends are presented in
 524 Table II for the achieved data rates. All the presented data rates
 525 are achieved below the FEC limit of 3.8×10^{-3} . The data rate
 526 decreases in the presence of solar irradiance. However, most
 527 of this reduction can be recovered using the blue filter. It is
 528 shown that a data rate of 1.015 Gb/s can be achieved under the
 529 presence of solar irradiance for the small APD in Scenario III.
 530 This is equivalent to a 10.4% reduction in data rate compared
 531 to Scenario I. This degradation can be reduced to 5.2% when
 532 the blue filter is used. A reduction of 24.75% in the data rates
 533 is witnessed in Scenario II for the large APD. This is improved
 534 to 4.73% when using the blue filter in Scenario II.

V. CONCLUSION

535
 536 VLC system is feasible in the presence of solar irradiance.
 537 Worst-case scenarios are considered in this study to prove the
 538 concept that VLC systems can work under the influence of
 539 strong solar irradiance. Shot noise caused by sunlight reduces
 540 the data rate of VLC systems. However, optical bandpass blue
 541 filters can limit the degradation caused by solar irradiance. Data
 542 rates above 1 Gb/s were experimentally achieved in the presence
 543 of solar irradiance without optical filtering. Simulation results
 544 have shown that an improvement of at least 6.47 dB can be
 545 achieved for SNR using off-the-shelf blue filters.

546 Saturation is a major drawback for photodiodes in the pres-
 547 ence of strong background noise. Automatic gain controller
 548 (AGC) can be used to reduce the likelihood of performance
 549 outage due to APD saturation. However, this is not considered
 550 in the current work and will be considered in future research.
 551 Bandpass optical filtering was considered as a technique to mit-
 552 igate solar irradiance noise. However, the results of this study
 553 can be used to build upon and to develop new solar irradiance
 554 noise mitigation techniques. An interesting solution could be
 555 envisaged to use angle-diversity receiver with signal combining
 556 techniques. However, the details of such investigation is out the
 557 scope of this paper and will be considered in future research.

APPENDIX A
 SOLAR POSITION

558

559 Three coordinate systems are used to calculate the position of
 560 the Sun: ecliptic coordinates; equatorial coordinates; and hori-
 561 zontal coordinates. These coordinate systems can be illustrated
 562 on the celestial sphere shown in Fig. 10. The parameters cor-
 563 responding to each coordinate system are mapped in Table III.
 564 The arbitrary coordinates in Fig. 10 is defined by Θ which is the
 565 angle between the principle and the projection of the Sun at the
 566 fundamental plane and by Ξ which is the angle between the Sun
 567 and the fundamental plane. Celestial coordinate systems can be
 568 converted into Cartesian coordinates using:

$$\begin{pmatrix} X \\ Y \\ Z \end{pmatrix} = \begin{pmatrix} \cos \Xi \cos \Theta \\ \cos \Xi \sin \Theta \\ \sin \Xi \end{pmatrix}. \quad (14)$$

569 The horizontal coordinate system is usually used for solar
 570 cell applications where the horizon of the observer is the funda-
 571 mental plane. The solar position can be projected on a celestial
 572 sphere using two angles: altitude Al and azimuth Az . The Earth
 573 revolves around the Sun in an elliptic orbit in which a complete
 574 revolution takes a year, a motion of around 1° per day. This mo-
 575 tion can be best described using the ecliptic coordinates where
 576 the principle is the position of the Sun during the spring equinox
 577 (the date of the year when the Earth's equator is alligned with
 578 the center of the Sun ecliptic). The angular ecliptic coordinates
 579 are the ecliptic longitude, λ and ecliptic latitude, β , which is
 580 given as $\beta \approx 0$ [18]. The ecliptic longitude can be given as [18]:

$$\lambda = q + 1.915^\circ \sin q + 0.020^\circ \sin 2q, \quad (15)$$

581 where q is the mean longitude given as [18]:

$$q = 280.459^\circ + 0.98564736^\circ D, \quad (16)$$

582 and g is the mean anomaly of the Sun, which accounts for the
 583 varying speeds of the Earth motion throughout the year. This is
 584 given as [18]:

$$g = 357.529^\circ + 0.98560028^\circ D, \quad (17)$$

585 where D is the time elapsed since the Greenwich noon of the
 586 1st of January 2000.

587 The equatorial coordinate system is required as a translational
 588 stage when transforming the ecliptic coordinates into horizontal
 589 coordinates, as follows:

$$\begin{pmatrix} X_{Equ} \\ Y_{Equ} \\ Z_{Equ} \end{pmatrix} = \begin{pmatrix} 1 & 0 & 0 \\ 0 & \cos \epsilon & -\sin \epsilon \\ 0 & \sin \epsilon & \cos \epsilon \end{pmatrix} \begin{pmatrix} X_{Ecl} \\ Y_{Ecl} \\ Z_{Ecl} \end{pmatrix}, \quad (18)$$

590 where ϵ is the axial tilt between the equatorial plane and the
 591 ecliptic plane. The axial tilt is zero in March and September
 592 equinox and takes its maximum value of $\pm 23.429^\circ$ in June
 593 and December solstices (the days when the maximum tilt is
 594 expernced at the north and south hemisphere, respectively).
 595 The axial tilt is given as [18]:

$$\epsilon = 23.429^\circ - 0.00000036^\circ D. \quad (19)$$

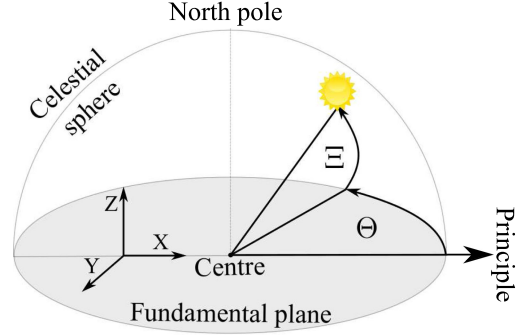


Fig. 10. An illustration of an arbitrary coordinate system on a celestial sphere.

TABLE III
 COORDINATION SYSTEMS CORRESPONDING PARAMETERS

Arbitrary	Ecliptic	Equatorial	Horizontal
center	center of the Earth	center of the Earth	observer
north pole	north ecliptic pole	north celestial pole	zenith
fundamental plane	ecliptic	celestial equator	horizon
principle	March equinox	March equinox	geographic north pole
Θ	ecliptic longitude (λ)	right ascension (α)	azimuth (Az)
Ξ	ecliptic latitude (β)	declination (δ)	altitude (Al)
$\begin{pmatrix} X \\ Y \\ Z \end{pmatrix}$	$\begin{pmatrix} X_{Ecl} \\ Y_{Ecl} \\ Z_{Ecl} \end{pmatrix}$	$\begin{pmatrix} X_{Equ} \\ Y_{Equ} \\ Z_{Equ} \end{pmatrix}$	$\begin{pmatrix} X_{Hor} \\ Y_{Hor} \\ Z_{Hor} \end{pmatrix}$

The equatorial coordinates are given by the right ascension α 596
 which is the angle between the March equinox and the projection 597
 of the Sun on the Earth's equator and by the declination δ which 598
 is the angle between the Sun and the Earth equator. The Sun 599
 moves 15° of longitude per hour. The hour angle is defined as 600
 the angle between the projection of the Sun on the fundamental 601
 plane and the meridian given at longitude of 0° (an imaginary 602
 circle passing through the north and south poles and the zenith 603
 of an observer). The hour angle is given by: 604

$$h = \theta_L - \alpha, \quad (20)$$

where θ_L is the angle between the meridian and the March 605
 equinox. It can also be defined as the local mean sidereal time 606
 (LMST). A sidereal day is the time that the Earth takes to com- 607
 plete a 360° rotation on its own axis. It is slightly shorter than 608
 the solar day mainly due to the rotation of the Earth around the 609
 Sun. The LMST can be given as: 610

$$\theta_L = \text{GMST} \frac{15^\circ}{\text{hour}} + \lambda_0, \quad (21)$$

where λ_0 is the longitude of the observer and GMST is the 611
 Greenwich mean sidereal time (GMST), which is defined as 612
 the hour angle between the March equinox and the meridian at 613
 Greenwich. GMST is calculated as [18]: 614

$$\text{GMST} = 18.697374558h + 24.06570982441908hD, \quad (22)$$

where it is scaled to values between 0 and 24.

615

616 The principle of the coordinates can be transformed from the
617 March equinox to the LMST using:

$$\begin{pmatrix} \cos \delta \cos h \\ \cos \delta \sin h \\ \sin \delta \end{pmatrix} = \begin{pmatrix} \cos \theta_L & \sin \theta_L & 0 \\ 3pt \sin \theta_L & -\cos \theta_L & 0 \\ 0 & 0 & 1 \end{pmatrix} \begin{pmatrix} X_{\text{Equ}} \\ Y_{\text{Equ}} \\ Z_{\text{Equ}} \end{pmatrix}, \quad (23)$$

618 In addition, the center of the coordinates can be transformed
619 from the center of the Earth to the position of the observer using:

$$\begin{pmatrix} X'_{\text{Hor}} \\ Y'_{\text{Hor}} \\ Z'_{\text{Hor}} \end{pmatrix} = \begin{pmatrix} \sin \phi_0 & 0 & -\cos \phi_0 \\ 0 & 1 & 0 \\ \cos \phi_0 & 0 & \sin \phi_0 \end{pmatrix} \begin{pmatrix} \cos \delta \cos h \\ \cos \delta \sin h \\ \sin \delta \end{pmatrix} \quad (24)$$

620 Following the prior calculations, the directions of X'_{Hor} and
621 Y'_{Hor} are directed towards south and west, respectively. The
622 following can be applied to adjust the reference direction to
623 north and east [18]:

$$\begin{pmatrix} X_{\text{Hor}} \\ Y_{\text{Hor}} \\ Z_{\text{Hor}} \end{pmatrix} = \begin{pmatrix} -1 & 0 & 0 \\ 0 & -1 & 0 \\ 0 & 0 & 1 \end{pmatrix} \begin{pmatrix} X'_{\text{Hor}} \\ Y'_{\text{Hor}} \\ Z'_{\text{Hor}} \end{pmatrix} \quad (25)$$

624 The horizontal coordinates can then be calculated using [18]:

$$\sin Al = \cos \phi_0 \cos \theta_L \cos \lambda_S + (\cos \phi_0 \sin \theta_L \cos \epsilon + \sin \phi_0 \sin \epsilon) \sin \lambda_S \quad (26)$$

$$\tan Az = \frac{\Gamma_1}{\Gamma_2 - \Gamma_3}, \quad (27)$$

625 where:

$$\Gamma_1 = -\sin \theta_L \cos \lambda_S + \cos \theta_L \cos \epsilon \sin \lambda_S, \quad (28)$$

$$\Gamma_2 = -\sin \phi_0 \cos \theta_L \cos \lambda_S, \quad (29)$$

$$\Gamma_3 = \sin \lambda_S (\sin \phi_0 \sin \theta_L \cos \epsilon - \cos \phi_0 \sin \epsilon), \quad (30)$$

REFERENCES

- 627 [1] Cisco Visual Networking Index, "Global mobile data traffic forecast
628 update, 2015-2020," CISCO, White Paper, Feb. 2016. [Online]. Available:
629 [http://www.cisco.com/c/en/us/solutions/collateral/service-provider/visu-
630 al-networking-index-vni/mobile-white-paper-c11-520862.pdf](http://www.cisco.com/c/en/us/solutions/collateral/service-provider/visual-networking-index-vni/mobile-white-paper-c11-520862.pdf)
- 631 [2] OFCOM report, "Award of the 2.3 and 3.4 GHz Spectrum Bands:
632 Competition issues and auction regulations," OFCOM, Consulta-
633 tion, Jan. 2017. [Online]. Available: [https://www.ofcom.org.uk/—
634 data/assets/pdf_file/0026/93545/award-of-the-spectrum-bands-
635 consultation.pdf](https://www.ofcom.org.uk/—data/assets/pdf_file/0026/93545/award-of-the-spectrum-bands-consultation.pdf)
- 636 [3] S. Dimitrov and H. Haas, *Principles of LED Light Communications: Tow-
637 ards Networked Li-Fi*. Cambridge, U.K.: Cambridge Univ. Press, 2015.
- 638 [4] M. S. Islim *et al.*, "Towards 10 Gb/s orthogonal frequency division
639 multiplexing-based visible light communication using a GaN violet micro-
640 LED," *Photon. Res.*, vol. 5, no. 2, pp. A35–A43, Apr. 2017. [Online].
641 Available: [http://www.osapublishing.org/prj/abstract.cfm?URI=prj-5-2-
642 A35](http://www.osapublishing.org/prj/abstract.cfm?URI=prj-5-2-A35)
- 643 [5] D. Tsonev, S. Videv, and H. Haas, "Towards a 100 Gb/s visible light
644 wireless access network," *Opt. Express*, vol. 23, no. 2, pp. 1627–1637,
645 Jan. 2015. [Online]. Available: [http://www.opticsexpress.org/abstract-
646 .cfm?URI=oe-23-2-1627](http://www.opticsexpress.org/abstract.cfm?URI=oe-23-2-1627)
- 647 [6] G. Povey, "Top 10 Li-Fi myths," Jun. 2012. [Online]. Available:
648 <http://visiblelightcomm.com/top-10-li-fi-myths/>
- 649 [7] M. S. Islim and H. Haas, "Modulation techniques for Li-Fi," *ZTE Com-
650 mun.*, vol. 14, no. 2, pp. 29–40, Apr. 2016.
- [8] Y. H. Chung and S. B. Oh, "Efficient optical filtering for outdoor visible
light communications in the presence of sunlight or artificial light,"
in *Proc. Int. Symp. Intell. Signal Process. Commun. Syst.*, Nov. 2013,
pp. 749–752.
- [9] T. Hamza, M.-A. Khalighi, S. Bourennane, P. Léon, and J. Opder-
becke, "Investigation of solar noise impact on the performance
of underwater wireless optical communication links," *Opt. Express*,
vol. 24, no. 22, pp. 25 832–25 845, Oct. 2016. [Online]. Available:
<http://www.opticsexpress.org/abstract.cfm?URI=oe-24-22-25832>
- [10] M. Beshr, C. Michie, and I. Andonovic, "Evaluation of visible light com-
munication system performance in the presence of sunlight irradiance," in
Proc. 2015 17th Int. Conf. Transp. Opt. Netw., Jul. 2015, pp. 1–4.
- [11] Y.-H. Kim and Y.-H. Chung, "Experimental outdoor visible light data
communication system using differential decision threshold with optical
and color filters," *Opt. Eng.*, vol. 54, pp. 1–3, 2015. [Online]. Available:
<http://dx.doi.org/10.1117/1.OE.54.4.040501>
- [12] D. R. Kim, S. H. Yang, H. S. Kim, Y. H. Son, and S. K. Han, "Outdoor
visible light communication for inter-vehicle communication using con-
troller area network," in *Proc. 2012 4th Int. Conf. Commun. Electron.*,
Aug. 2012, pp. 31–34.
- [13] ASTM, *Standard Tables for Reference Solar Spectral Irradiances: Direct
Normal and Hemispherical on 37 Tilted Surface*, Standard ASTM-G173-
03, 2014. [Online]. Available: <https://doi.org/10.1520/G0173-03R12>
- [14] M. Islim and H. Haas, "An investigation of the sunlight irradiance ef-
fect on visible light communications," in *Proc. 27th Int. Symp. Pers.
Indoor Mobile Radio Commun.*, Montreal, QC, Canada, Oct. 8–13,
2017, pp. 1–6.
- [15] G. Cossu *et al.*, "Experimental demonstration of high speed underwater
visible light communications," in *Proc. 2013 2nd Int. Workshop Opt.
Wireless Commun.*, Oct. 2013, pp. 11–15.
- [16] ASTM, *Standard Solar Constant and Zero Air Mass Solar Spectral Ir-
radiance Tables*, Standard ASTM-E490-00a, 2014. [Online]. Available:
<https://doi.org/10.1520/E0490>
- [17] W. B. Stine and M. Geyer, *Power From the Sun*, 2001. [Online]. Available:
<http://Powerfromthesun.net>
- [18] A. Smets, K. Jäger, O. Isabella, M. Zeman, and R. van Swaaij, *Solar
Energy: The Physics and Engineering of Photovoltaic Conversion, Tech-
nologies and Systems*. Cambridge, U.K.: UIT Cambridge, 2016. [Online].
Available: <https://books.google.co.uk/books?id=vTkdgEACAAJ>
- [19] I. Reda and A. Andreas, "Solar position algorithm for solar radiation
applications," *Sol. Energy*, vol. 76, no. 5, pp. 577–589, 2004.
- [20] C. A. Gueymard, "Parameterized transmittance model for direct beam and
circumsolar spectral irradiance," *Sol. Energy*, vol. 71, no. 5, pp. 325–346,
2001.
- [21] C. Gueymard, *SMARTS2: A Simple Model of the Atmospheric Radiative
Transfer of Sunshine: Algorithms and Performance Assessment*. Cocoa,
FL, USA: Florida Solar Energy Center, 1995.
- [22] S. Rajbhandari *et al.*, "A review of gallium nitride LEDs for multi-
gigabit-per-second visible light data communications," *Semicond. Sci.
Technol.*, vol. 32, no. 2, 2017, Art. no. 023001. [Online]. Available:
<http://stacks.iop.org/0268-1242/32/i=2/a=023001>
- [23] F. Xu, M. A. Khalighi, and S. Bourennane, "Impact of different noise
sources on the performance of PIN- and APD-based FSO receivers," in
Proc. 11th Int. Conf. Telecommun., Jun. 2011, pp. 211–218.
- [24] R. Rondanelli, A. Molina, and M. Falvey, "The Atacama surface solar
maximum," *Bull. Amer. Meteorol. Soc.*, vol. 96, no. 3, pp. 405–418, 2015.
[Online]. Available: <https://doi.org/10.1175/BAMS-D-13-00175.1>
- [25] S. Dimitrov, S. Sinanovic, and H. Haas, "Signal shaping and modulation
for optical wireless communication," *J. Lightw. Technol.*, vol. 30, no. 9,
pp. 1319–1328, May 2012.
- [26] F. M. Davidson and X. Sun, "Gaussian approximation versus nearly ex-
act performance analysis of optical communication systems with PPM
signaling and APD receivers," *IEEE Trans. Commun.*, vol. 36, no. 11,
pp. 1185–1192, Nov. 1988.
- [27] Hamamatsu Photonics K.K., "Characteristics and Use of SI-
APD (avalanche photodiode)," May 2004. [Online]. Available:
[http://neutron.physics.ucsb.edu/docs/Characteristics_and_use_of_SI-
APD.pdf](http://neutron.physics.ucsb.edu/docs/Characteristics_and_use_of_SI-APD.pdf)
- [28] G. Keiser, *Optical Communications Essentials*. New York, NY, USA:
McGraw-Hill, 2003.
- [29] J. M. Kahn and J. R. Barry, "Wireless infrared communications," *Proc.
IEEE*, vol. 85, no. 2, pp. 265–298, Feb. 1997.
- [30] H. E. Levin, "A complete and optimal data allocation method for practical
discrete multitone systems," in *Proc. IEEE Global Telecommun. Conf.*,
San Antonio, TX, USA, Nov. 25–29, 2001, vol. 1, pp. 369–374.

- 726 [31] C. Shannon, "A mathematical theory of communication," *Bell Syst. Tech. J.*, vol. 27, pp. 379–423 & 623–656, Jul./Oct. 1948.
- 727
- 728 [32] S. Dimitrov and H. Haas, "Information rate of OFDM-based optical wire-
729 less communication systems with nonlinear distortion," *IEEE J. Lightw. Technol.*, vol. 31, no. 6, pp. 918–929, Mar. 2013.
- 730
- 731 [33] F. Xiong, *Digital Modulation Techniques*, 2nd ed. Norwood, MA, USA: Artech House, 2006.
- 732
- 733 [34] C. M. Lampert, "Heat mirror coatings for energy conserving windows," *Sol. Energy Mater.*, vol. 6, no. 1, pp. 1–41, 1981. [Online]. Available: <http://www.sciencedirect.com/science/article/pii/0165163381900472>
- 734
- 735 [35] E. Diaz and M. Knobl, "Prototyping illumination systems with stock
736 optical components," *Photonik Int.*, Fellbach, Germany, 2012.
- 737

738 **Mohamed Sufyan Islim** (S'07) received the M.Sc. degree (distinction) in com-
739 munications engineering from Aleppo University, Aleppo, Syria, in 2013, and
740 the M.Sc. degree (distinction) in signal processing and communications, from
741 the University of Edinburgh, Edinburgh, U.K., in 2014. He is currently working
742 toward the Ph.D. degree at the LiFi Research and Development Centre, Uni-
743 versity of Edinburgh. His research interests include optical OFDM, LiFi, and
744 optical wireless communications. Among several scholarships he was awarded
745 in 2013, he was the recipient of the Global Edinburgh Syrian Scholarship from
746 Edinburgh University. He also received the 2014 IEEE communications chapter
747 prize for the best master project.

748

749 **Stefan Videv**, biography not available at the time of publication.

750

751 **Majid Safari** (S'08–M'11) received the B.Sc. degree in electrical and computer
752 engineering from the University of Tehran, Tehran, Iran, in 2003, the M.Sc. de-
753 gree in electrical engineering from Sharif University of Technology, Tehran,
754 Iran, in 2005, and the Ph.D. degree in electrical and computer engineering from
755 the University of Waterloo, Waterloo, ON, Canada, in 2011.

756 He is currently an Assistant Professor with the Institute for Digital Commu-
757 nications, University of Edinburgh, Edinburgh, U.K. Before joining Edinburgh
758 in 2013, he was a postdoctoral fellow with McMaster University, Hamilton,
759 ON, Canada. His main research interest is the application of information theory
760 and signal processing in optical communications including fiber-optic commu-
761 nication, free-space optical communication, visible light communication, and
762 quantum communication.

763 Dr. Safari is currently an Associate Editor for the IEEE COMMUNICATION
764 LETTERS and was the TPC co-chair for the 4th International Workshop on Op-
765 tical Wireless Communication in 2015.

766

767 **Enyuan Xie** received the Ph.D. degree in physics from the University of Strath-
768 clyde, Glasgow, U.K., in 2013. Since then, he has been with the Institute of
769 Photonics, University of Strathclyde, Glasgow, U.K., as a research fellow, be-
770 coming involved in the fabrication, characterization, and application of GaN-
771 based micro-LED arrays.

772

773 **Jonathan J. D. McKendry** received the M.S. degree in electronics and electrical
774 engineering from the University of Glasgow, Glasgow, U.K., in 2006, and the
775 Ph.D. degree from the University of Strathclyde, Glasgow, U.K., in 2011. In
776 2007, he joined the Institute of Photonics as a Ph.D. student where the focus of his
777 Ph.D. was on the application of AlInGaN-based micro-LEDs for time-resolved
778 fluorescence lifetime measurements and optical communications. He currently
779 works as a Research Associate with the Institute of Photonics, University of
780 Strathclyde, Glasgow, U.K., primarily on the subject of LED-based visible light
781 communications. To date, he has authored or co-authored more than 30 peer-
782 reviewed journal articles and 30 conference submissions.

783

Erdan Gu received the Ph.D. degree in thin film physics from Aberdeen Uni-
784 versity, U.K., in 1992. Afterward, he was a Research Fellow with the Cavendish
785 Laboratory, Cambridge University, Cambridge, U.K. In 1997, he joined the Thin
786 Film Group, Oxford Instruments plc, U.K. as a Senior Research Scientist work-
787 ing on superconducting photonic devices. Since July 2002, he has been with the
788 Institute of Photonics, University of Strathclyde, Glasgow, U.K., where he is an
789 Associate Director and a Research Team Leader. In the Institute of Photonics,
790 he is working and playing a leading role in a range of research projects on pho-
791 tonic materials and devices, micro/nano optoelectronics, diamond photonics,
792 and optoelectronic devices for visible light communications.

793

794

Martin D. Dawson (M'85–SM'98–F'09) is a physicist known for his work
795 on lasers and compound semiconductors. He is the Director of Research with
796 the Institute of Photonics, University of Strathclyde, Glasgow, U.K., which he
797 helped establish 20 years ago, and he was also appointed Inaugural Head of
798 the Fraunhofer Centre for Applied Photonics in October 2012. He has more
799 than 30 years' experience of applied research gained in academia and industry
800 in the U.K. and USA, and he has been involved in the formation and technical
801 development of a number of spin-out businesses, most recently including mLED
802 Ltd. He holds an EPSRC Programme Grant on visible light communications
803 and gave a Rank Prize Lecture in 2014 on applied research in photonics. He was
804 the recipient of the 2016 Gabor Medal and Prize by the Institute of Physics and
805 the 2016 Aron Kessel Award by the IEEE Photonics Society.

806

807

Harald Haas (S'98–AM'00–M'03–SM'17–F'18) received the Ph.D. degree
808 from the University of Edinburgh, Edinburgh, U.K., in 2001. He is currently the
809 Chair of Mobile Communications, University of Edinburgh, and the Founder
810 and Chief Scientific Officer of pureLiFi Ltd. pureLiFi Ltd has more than 50
811 employees and has operations in the USA and Singapore. He is also the Direc-
812 tor of the LiFi Research and Development Center, University of Edinburgh. His
813 main research interests include optical wireless communications, hybrid optical
814 wireless and RF communications, spatial modulation, and interference coordi-
815 nation in wireless networks. He first introduced and coined spatial modulation
816 and LiFi. LiFi was listed among the 50 best inventions in TIME Magazine 2011.
817 He was an invited speaker at TED Global 2011, and his talk: "Wireless Data
818 from Every Light Bulb" has been watched online more than 2.5 million times.
819 He gave a second TED Global lecture in 2015 on the use of solar cells as LiFi
820 data detectors and energy harvesters. This has been viewed online more than
821 2.0 million times. He holds 43 patents and has more than 30 pending patent
822 applications. He has published more than 400 conference and journal papers
823 including a paper in *Science*. His Google Scholar h-index is 67, and his works
824 have been cited more than 19,000 times. He was on the Thomson Reuters list
825 of highly cited scientists, 2017. He co-authors a book entitled: "*Principles of
826 LED Light Communications Towards Networked Li-Fi*" (Cambridge University
827 Press, Cambridge, U.K., 2015).

828

829 Prof. Haas is an editor for the IEEE TRANSACTIONS ON COMMUNICATIONS
830 and the IEEE JOURNAL OF LIGHTWAVE TECHNOLOGY. He was the co-recipient
831 of the recent Best Paper Awards at VTC-Fall, 2013, VTC-Spring 2015, ICC
832 2016, and ICC 2017. He was the co-recipient of the EURASIP Best Paper
833 Award for the *Journal on Wireless Communications and Networking* in 2015
834 and co-recipient of the Jack Neubauer Memorial Award of the IEEE Vehicular
835 Technology Society. He is the recipient of the Tam Dalyell Prize 2013 awarded
836 by the University of Edinburgh for excellence in engaging the public with sci-
837 ence. In 2016, he was the recipient of the Outstanding Achievement Award
838 from the International Solid State Lighting Alliance, which was awarded to him
839 by Prof. Shuji Nakamura. He has delivered 50 keynote talks at international
840 conferences and workshops. In 2012, he was the recipient of the prestigious
841 Established Career Fellowship from the Engineering and Physical Sciences Re-
842 search Council within information and communications technology in the U.K.
843 In 2014, he was selected by EPSRC as one of ten recognising inspirational
844 scientists and engineers (RISE) Leaders in the U.K. He was elected a Fellow of
845 the Royal Society of Edinburgh in 2017.

846